Erschienen in: Chemical Communications ; 56 (2020), 92. - S. 14439-14442.
https://dx.doi.org/10.1039/D0CC04628K

Synthesis of nickel hexacyanoferrate nanocubes with tuneable dimensions *via* temperature-controlled Ni^{2+}-citrate complexation

Sascha Keßler, Guillermo González-Rubio, Elrike Rea Reinalter, Michael Kovermann and Helmut Cölfen *

The citrate-assisted growth of nickel hexacyanoferrate (NiHCF) nanocubes was investigated. Control over the complexation of Ni^{2+} ions with citrate at different temperatures enabled fine tuning of the nanocrystal (NC) dimensions and their self-assembly into mesocrystals. Our results introduce new concepts towards the synthesis of NiHCF NCs, potentially applicable to other members of the Prussian blue analogues family.

In recent decades, the interest in Prussian blue analogues (PBAs) has steadily increased due to their potential as cost-effective alternative and environmentally friendly materials for catalysis, metal-ion batteries, supercapacitors, or CO_2 adsorption.[1–5] PBAs belong to an appealing class of low-density compounds with a generic formula of $A_xM[M'(CN)_6]_y{\cdot}nH_2O$ ($0 \leq x \leq 2$; $0 < y \leq 1$), where M and M′ are both high spin and low spin transition metals (*i.e.*, typically Mn, Fe Co, Ni, Cu, or Zn), and A is an alkali metal (*e.g.*, Li, Na, or K) that ensures neutrality.[6] Both transition metals are then connected by $C{\equiv}N^-$ ligands, giving rise to highly stable open structures with tuneable size pores and vast internal surface areas. As a result, they can intercalate metal ions while preserving their crystalline structure. Depending on the nature of the transition metal and its oxidation state, an array of PBAs with distinct magnetic, optical and electrical behaviour can be obtained.[7]

Besides the chemical composition, the dimensions of PBA crystals also play a critical role in determining their behavior, being typically superior when their size is reduced to the nanoscale due to the appearance of surface effects. For instance, it is possible to improve their catalytic activity and molecular adsorption kinetics when using nanosized PBAs.[8] Moreover, they can be exploited as building blocks for the formation of hierarchical structures with unique properties, distinct to that of the constituents or the bulk. In this case, the shape of the NCs determines the nature of the assembled structure. Hence, the development of optimized methods for their synthesis with desired chemical composition, shape and size emerges pivotal for the implementation of PBAs in technology.

The synthesis of bulk PBAs is typically performed *via* a co-precipitation method, which relies on the direct reaction of M′ metal precursor with $A_x[M'(CN)_6]$ in an aqueous solution.[9] Nevertheless, the insolubility of PBAs naturally renders low control over their NC growth. Among different approaches explored to govern the co-precipitation process (*e.g.*, crystallization inside porous scaffolds or soft templates such as nanodroplets), the addition of organic additives such as citrate has emerged as one of the most elegant synthetic pathways, enabling the homogeneous growth of PBA nanoparticles with tuneable dimensions.[10–12] Although, it is known that the improved PBAs synthesis in the presence of citrate is probably related to the formation of M-citrate coordination complexes, a complete understanding of the growth mechanism remains elusive. As a direct consequence, the potential of citrate for the synthesis of PBAs remains unexploited. For instance, the strength of the metal ion-citrate association varies as a function of temperature according to the Van't Hoff equation, implying that it may be used to tailor the PBAs growth.[13] Indeed, It has been shown, that the presence of citrate can influence the particle size of PBA NCs.[14]

In this work, we aimed at investigating the interplay between citrate and temperature in the growth of cubic PBA NCs with distinct dimensions. Among the variety of PBAs, we focused on NiHCF, an appealing material that holds great prospects for earth-abundant metal-ion batteries or heterogeneous catalyst.[4,15] Moreover, it may serve as a model system to investigate the synthesis of more complex PBAs. Thus, we first investigated the co-precipitation of NiHCF nanoparticles in the absence and presence of citrate. The synthesis was performed by direct mixing of two aqueous solutions (40 mL) containing potassium hexacyanoferrate(III) (0.02 M) and nickel(II) acetate (0.03 M),

Physical Chemistry, Department of Chemistry, University of Konstanz, Universitätsstrasse 10, D-78457 Konstanz, Germany.
E-mail: Helmut.Cölfen@Uni-Konstanz.de

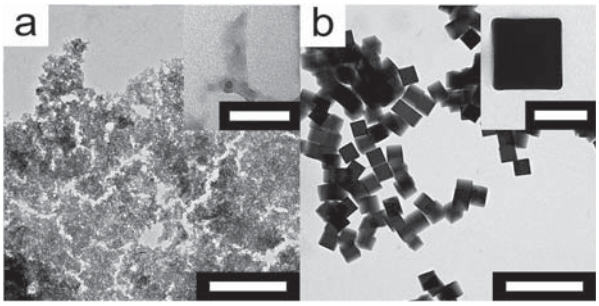

Fig. 1 Effect of citrate on NiHFC synthesis. (a and b) Transmission electron microscopy (TEM) images of NiHCF nanoparticles obtained in the absence (a) and presence (b) of citrate. Scale bars: 500 nm, 50 nm (inset a), and 100 nm (insets b).

respectively. When the reaction was completed in the presence of citrate ions, its trisodium salt was introduced in the Ni^{2+} solution prior to mixing with hexacyanoferrate (HCF) solution. Analysis of the products *via* TEM revealed the occurrence of single-crystal 133 nm cubic and sub 15 nm NCs with undefined shape depending on whether citrate was present or absent in the growth mixture, respectively (Fig. 1a and b). Both products were found to crystallize in the same cubic structure (Fig. S1 ESI;† *i.e.*, $F\bar{4}3m$) with a corresponding elemental composition of $Na_{0.125}Ni_{2.875}[Fe(CN)_6]_2{\cdot}14.7H_2O$ for the 133 nm NCs and $K_{0.14}Ni_{2.86}[Fe(CN)_6]_2{\cdot}23.5H_2O$ for the sub 15 nm NCs (Fig. S2, ESI†). These results indicate that citrate can significantly modify the dimensions and morphology of the synthesized NiHCF NCs.[14]

On the one hand, the synthesis of NC colloids often requires the use of surface ligands to control the growth process and to maintain their colloidal stability. Nevertheless, in our case, analysis of IR spectra of NiHCF prepared in the presence of citrate did not reveal bands characteristic for citrate (Fig. S3, ESI†), indicating that the interaction of citrate with NiHCF might be too weak to impact the formation of NiHCF NCs. The rate constant of NC formation (*via* co-precipitation) is strongly dependent on the degree of solution supersaturation. Due to poor solubility of NiHCF, high supersaturation levels can be easily reached even at low concentrations. In this context, citrate can form coordination complexes with different transition metals including Ni. This phenomenon could decrease the concentration of free metal ions in solution (*i.e.*, lowering the supersaturation), eventually leading to fewer nuclei forming and the growth of larger NCs. To validate this hypothesis, we investigated the formation of Ni^{2+}-citrate (NiCit) complex in the presence of HCF. In this regard, one-dimensional ^{1}H-NMR experiments were conducted to unveil the dynamics of NiCit interaction during the NiHCF NCs synthesis (Fig. S3, ESI†). When citrate is not coordinated to metals at a pH value ranging between 6.5 and 7 (*i.e.*, it decreases from 6.8 to 6.5 during the synthesis, Fig. S4, ESI†), it exhibits two characteristic doublets in the 2.8–2.5 ppm range corresponding to the citrate monoprotonated species ($HCit^{2-}$).[16] After the addition of Ni^{2+}, a decreased broadening of the citrate signal intensity was observed, pointing out the formation of a NiCit complex.[17] Indeed, complete complexation of citrate should lead to the total disappearance of this signal. However, as a 50% excess of citrate was present in the mixture, only a fraction of citrate molecules was coordinated with metal ions (*i.e.*, Fig. S5 and S6 ESI;† NiCit stoichiometry determined *via* conductivity measurements and NMR spectroscopy was 1 : 1.06 while a [citrate] : [Ni^{2+}] = 1.5 was used during the synthesis). Subsequently, HCF solution was injected and the ^{1}H-NMR resonance signals of citrate were monitored. A significant recovery of the intensity of resonance signals comprising citrate was noticed after 24 h, which was probably caused by the disappearance of the Ni^{2+} complex due to precipitation of the metal ions from solution. Overall, these results strongly indicate that the NiCit complex is stable for several hours in the presence of HCF. As a consequence, the effective concentration of Ni^{2+} is likely much lower than in the absence of citrate molecules, thereby lowering the supersaturation. It is important to underline that a decrease in the concentration of free Ni^{2+} may also affect the growth kinetics.

Besides tuning of the particle size *via* the citrate concentration, a precise kinetic control of the nucleation and growth process is a principle further possibility. To investigate this hypothesis, we monitored the changes in the turbidity of the growth mixture during the nanoparticle synthesis (*i.e.*, turbidity rises once nucleation begins). Thus, in the absence of citrate, the nucleation and subsequent growth were found to occur in a few minutes, as indicated by the fast increment of the solution turbidity that saturates the instrument. On the contrary, the onset of nucleation was significantly delayed in the presence of citrate (Fig. S7, ESI†), pointing out a substantial modification of the speed of growth. Considering the strong dependence of growth kinetics on the size of the NiHCF NCs (Fig. 1a and b), obtaining full control of this process should provide access to NC with tuneable dimensions. It is important to underline that the speed of NC growth depends on the NiCit complexation, which is an endothermic process.[18] As such, the tuning of the growth temperature may emerge as a simple strategy to modify the growth kinetics and, consequently, the NiHCF dimensions.

The synthesis of NiHCF was performed at different temperatures to explore this idea. We found that the growth time was significantly delayed at temperatures below 25 °C and increased at temperatures above 25 °C (Fig. 2a). Analysis of TEM micrographs taken from products revealed that the smallest NCs were formed at temperatures below 25 °C, whereas an increase of the size was identified for those NiHCF NCs prepared at higher temperatures. Therefore, NiHCF NCs of 78 nm were grown at 0 °C, while sizes of 96, 133, 147, 223, 231 and 538 nm were reached at 10, 25, 35, 50, 70 and 90 °C, respectively (Fig. 2b–f and Fig. S8, ESI†). Overall, these results successfully reveal the critical role of the co-precipitation kinetics in the formation of NiHCF NCs. Moreover, in the presence of citrate, the synthesis can be controlled *via* the growth temperature, enabling the formation of NiHCF NCs with tuneable dimensions and size dispersity below 8% (between 10 and 35 °C, Fig. S8, ESI†). Note, when the temperature was not controlled, the oscillation of the room temperature gave rise to a decrease of the NiHCF NC quality (Fig. S9, ESI†).

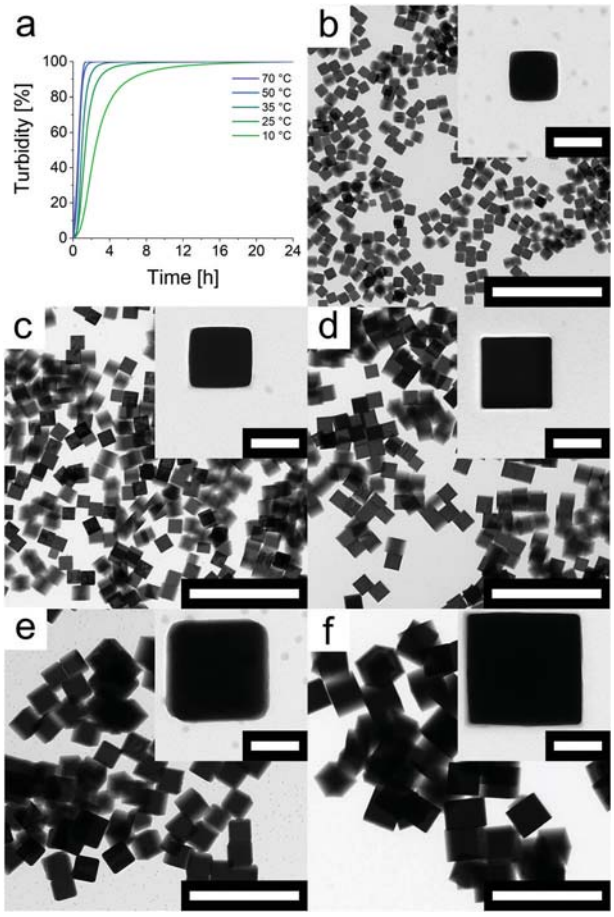

Fig. 2 Growth kinetics and tuneability of NiHCF NC dimensions. (a) Time course of the turbidity during the synthesis of NiHCF performed at different temperatures. (b–f) TEM micrographs of NiHCF with distinct dimensions: 96 ± 8.3 nm at 10 °C, 133 ± 8.0 nm at 25 °C, 147 ± 8.0 nm at 35 °C, 223 ± 26 nm at 50 °C and 231 ± 44 nm at 70 °C. Scale bars: 1 μm and 100 nm (insets).

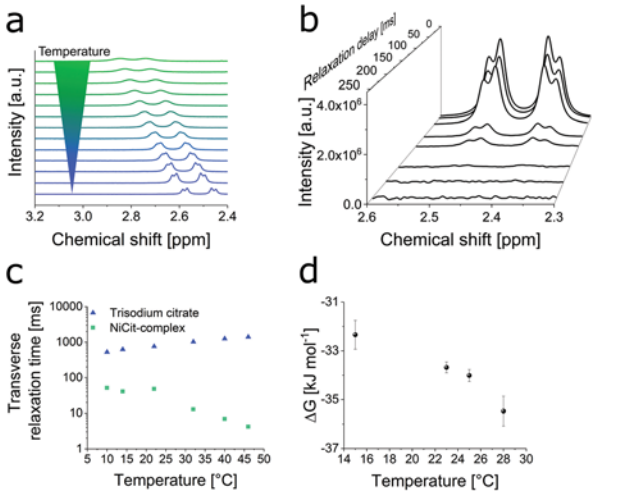

Fig. 3 Temperature dependence of the association process between Ni^{2+} and citrate. (a) ^{1}H-NMR spectra of citrate in the presence of Ni^{2+} recorded at different temperatures ranging from 10 °C (blue) to 46 °C (green). Chemical shift of the citrate resonance signal occurs from temperature-dependent shift of the water reference signal. (b) Dependence of signal intensity in NMR spectra on the relaxation delay applied in Carr–Purcell–Meiboom–Gill (CPMG)-experiments to obtain the transverse relaxation time (T_2). (c) Dependence of T_2 of citrate (blue triangle) and NiCit complex (green triangle) on the temperatures. (d) Dependence of Gibbs' free energy on temperature derived from isothermal titration calorimetry (ITC) measurements.

To gain insights into the role of citrate and the nature of the NiCit association at different temperatures, at a molecular level, the thermodynamic stability of the complex was investigated by applying one-dimensional ^{1}H-NMR spectroscopy (note that the proton resonance signals compromising citrate are sensitive to the binding strength). Thereby, a substantial decrease in signal intensity in resonance belonging to citrate was noted, suggesting that a stronger interaction of citrate with Ni^{2+} occurs at elevated temperatures (Fig. 3a). These results indicated that the chemical equilibrium was shifted towards the NiCit complex formation. Further investigation of this phenomenon was accomplished using the Carr–Purcell–Meiboom–Gill (CPMG) experiment to determine the T_2 of the Ni^{2+}-citrate-complex at different temperatures.[19] In a typical CPMG-based NMR experiment, the decay of a signal intensity is monitored by applying an increasing relaxation delay in order to obtain T_2 (Fig. 3b). In the case of the Ni^{2+}-citrate-complex, we observed a substantial decrease in T_2 of the resonance signal at 2.38 ppm as the temperature was increased from 10 °C to 46 °C (Fig. 3c and Fig. S10, ESI†). Although T_2 may rise due to an increase in molecular dynamics induced by elevated temperatures (as observed for free citrate), a stronger interaction with paramagnetic Ni^{2+} can reverse this effect significantly.[20] Thus, the observed dependence of T_2 on increasing temperature revealed that NiCit interactions become more pronounced, qualitatively supporting that the chemical equilibrium shifted towards the complex formation (Fig. S11 and S12, ESI†). Finally, ITC was employed to quantitatively determine the thermodynamics variables of the NiCit complexation process (Fig. 3d and Fig. S13, ESI†). We observed a noticeable decrease in the Gibbs' free energy of complex formation when the temperature was raised (from 32.3 kJ mol^{-1} at 15 °C to 35.5 kJ mol^{-1} at 28 °C), thereby providing additional evidence of the enhanced stability of the NiCit complex at high temperatures (Fig. 3d).

Finally, the self-assembly of NiHCF NCs into highly ordered superstructures (mesocrystal) was investigated. The use of high quality NCs is an essential prerequisite in the construction of hierarchical structures with tailored physical–chemical properties, as they can be more structured into ordered arrangements. Owing to the low size and shape dispersity of the obtained NiHCF NCs, they were found to easily self-assemble into micron-sized mesocrystals *via* gas diffusion of an antisolvent into a water-based dispersion of the NCs.[21] In a typical setup, a double-polished Si-wafer was placed inside a small glass tube filled with the NC dispersion. This glass tube was situated inside a glass vial containing the antisolvent (ethanol). The mesocrystals are formed by a continuous decrease of the dispersion's colloidal stability within 14 days. The morphology of the precipitated microstructures grown on the Si-wafer was characterized *via* SEM, which revealed the formation of mesocrystalline

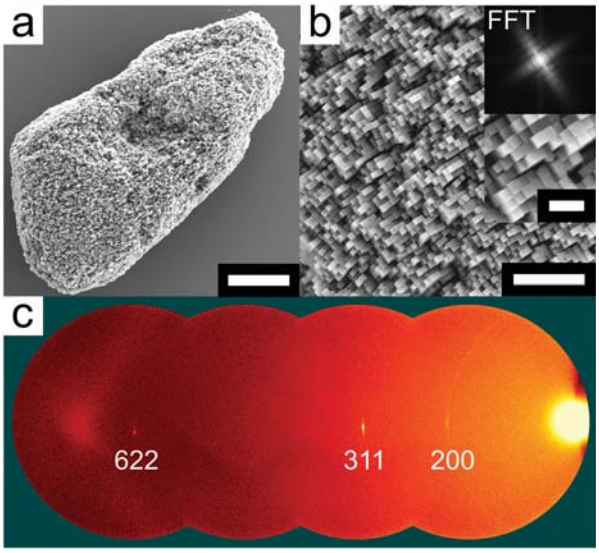

Fig. 4 Self-assembly of NiHCF NCs into mesocrystals. (a) Low magnification and (b) high magnification scanning electron microscopy (SEM) images of NiHCF mesocrystal composed with 176 nm NCs, and their corresponding FFT (inset top right). (c) Wide angle X-ray scattering (WAXS) pattern with sharp Bragg peaks of the [622], [311] and [200] lattice planes. (Scale bar: 5.0 μm (top left) and 2.0 μm, inset 500 nm (top right)).

structures (Fig. 4a and b). In addition, WAXS confirmed the formation of a mesocrystalline structure due to the existence of sharp Bragg peaks. These are characteristic for type I mesocrystals with a longe-range order on the atomic scale.[22]

In summary, we have investigated the role of citrate in the co-precipitation of NiHCF NCs with narrow size and shape distributions. In the presence of citrate, Ni^{2+} is chelated by citrate, a process that was found to occur also in the presence of the precursor KHCF. A decrease of free Ni^{2+} available for the formation of NiHCF is thus produced, which lowers both the supersaturation and the growth kinetics. Moreover, the extent of the NiCit complexation process is greatly improved at high temperature, as revealed by ^{1}H-NMR and ITC experiments. As a result, the interplay between the presence of citrate and the growth temperature enables extended control over the growth kinetics, leading to NiHCF NCs with tailored dimensions. Owing to the high quality of the obtained NiHCF NCs, their self-assembly into hierarchically ordered mesocrystalline structures was easily achieved. These results represent an appealing example regarding the understanding of the role of citrate in the synthesis of PBAs and can therefore lead to the development of reliable and reproducible synthetic protocols. Moreover, due to the ability of citrate to chelate an array of transition metals, the reported strategy could be potentially expanded to the synthesis of other nanoparticles of the PBAs family where the co-precipitation method is typically employed.

This work was funded by the Deutsche Forschungsgemeinschaft (Grant CO194/16-1). We thank the ''Particle Analysis Center'' of the University of Konstanz for the PXRD and WAXS measurements. Furthermore, the authors thank the ''Nanostructure Laboratory'' for providing SEM measurement time and we also thank Anke Friemel from the ''NMR Core Facility'' of the University of Konstanz for experimental support. G. González-Rubio gratefully acknowledges the Alexander von Humboldt Foundation for financial support.

Conflicts of interest

There are no conflicts to declare.

Notes and references

1 L. Hu, R. Zhang, L. Wei, F. Zhang and Q. Chen, *Nanoscale*, 2015, **7**, 450–454.
2 Y. Du, J. Chen, L. Li, H. Shi, K. Shao and M. Zhu, *ACS Sustainable Chem. Eng.*, 2019, 7(15), 13523–13531.
3 L. Hu, P. Zhang, Q.-W. Chen, J.-Y. Mei and N. Yan, *RSC Adv.*, 2011, **1**, 1574–1578.
4 C. D. Wessells, M. T. McDowell, S. V. Peddada, M. Pasta, R. A. Huggins and Y. Cui, *ACS Nano*, 2012, **6**, 1688–1694.
5 Y. Z. Zhang, T. Cheng, Y. Wang, W. Y. Lai, H. Pang and W. Huang, *Adv. Mater.*, 2016, **28**, 5242–5248.
6 Y. Tang, W. Li, P. Feng, M. Zhou, K. Wang, Y. Wang, K. Zaghib and K. Jiang, *Adv. Funct. Mater.*, 2020, **30**, 1908754.
7 Y. Ru, S. Zheng, H. Xue and H. Pang, *Chem. Eng. J.*, 2019, 122853.
8 X. Zhou, W. Xu, G. Liu, D. Panda and P. Chen, *J. Am. Chem. Soc.*, 2009, **132**, 138–146.
9 Y. Song, J. He, H. Wu, X. Li, J. Yu, Y. Zhang and L. Wang, *Electrochim. Acta*, 2015, **182**, 165–172.
10 A. Azhar, Y. Li, Z. Cai, M. B. Zakaria, M. K. Masud, M. S. A. Hossain, J. Kim, W. Zhang, J. Na and Y. Yamauchi, *Bull. Chem. Soc. Jpn.*, 2019, **92**, 875–904.
11 M. Hu, S. Ishihara, K. Ariga, M. Imura and Y. Yamauchi, *Chem. – Eur. J.*, 2013, **19**, 1882–1885.
12 F. Shiba, R. Fujishiro, T. Kojima and Y. Okawa, *J. Phys. Chem. C*, 2012, **116**, 3394–3399.
13 P. Atkins and J. De Paula, *Atkins' physical chemistry*, 2006, pp. 223–226.
14 Y. D. Chiang, M. Hu, Y. Kamachi, S. Ishihara, K. Takai, Y. Tsujimoto, K. Ariga, K. C. W. Wu and Y. Yamauchi, *Eur. J. Inorg. Chem.*, 2013, 3141–3145.
15 P. Chandra, M. Latwal, V. K. Bansal and S. P. Singh, *Chin. J. Catal.*, 2011, **32**, 1844–1849.
16 O. Y. Zelenin, *Russ. J. Coord. Chem.*, 2007, **33**, 346–350.
17 K. E. Schwarzhans, *Angew. Chem., Int. Ed. Engl.*, 1970, **9**, 946–953.
18 D. Wyrzykowski and L. Chmurzyński, *J. Therm. Anal. Calorim.*, 2009, **102**, 61–64.
19 M. Kovermann, R. Zierold, C. Haupt, C. Löw and J. Balbach, *Biochim. Biophys. Acta, Proteins Proteomics*, 2011, **1814**, 873–881.
20 J. J. Led and D. M. Grant, *J. Am. Chem. Soc.*, 1977, **99**, 5845–5858.
21 J. Opel, J. Brunner, E. Sturm, M. Kellermeier, H. Cölfen and J. M. García-Ruiz, *Adv. Funct. Mater.*, 2019, **29**, 1902047.
22 L. Bergström, E. V. Sturm, G. Salazar-Alvarez and H. Cölfen, *Acc. Chem. Res.*, 2015, **48**, 1391–1402.